FeCoCp$_3$ Molecular Magnets as Spin Filters

P.N. Abufager,[*,†] R. Robles,[†] and N. Lorente[*,†]

ICN2 - Institut Catala de Nanociencia i Nanotecnologia, Campus UAB, E-08193 Bellaterra (Barcelona), Spain, Instituto de Física de Rosario, Consejo Nacional de Investigaciones Científicas y Técnicas (CONICET) and Universidad Nacional de Rosario, Av. Pellegrini 250 (2000) Rosario, Argentina, Centro de Física de Materiales CFM/MPC (CSIC-UPV/EHU), Paseo Manuel de Lardizabal 5, 20018 Donostia-San Sebastián, Spain, and Donostia International Physics Center (DIPC), Paseo Manuel de Lardizabal 4, 20018 Donostia-San Sebastián, Spain

E-mail: abufager@ifir-conicet.gov.ar; nicolas_lorente001@ehu.eus

---

[*]To whom correspondence should be addressed

[†]ICN2 - Institut Catala de Nanociencia i Nanotecnologia, Campus UAB, E-08193 Bellaterra (Barcelona), Spain

[‡]Instituto de Física de Rosario, Consejo Nacional de Investigaciones Científicas y Técnicas (CONICET) and Universidad Nacional de Rosario, Av. Pellegrini 250 (2000) Rosario, Argentina

[¶]Centro de Física de Materiales CFM/MPC (CSIC-UPV/EHU), Paseo Manuel de Lardizabal 5, 20018 Donostia-San Sebastián, Spain

[§]Donostia International Physics Center (DIPC), Paseo Manuel de Lardizabal 4, 20018 Donostia-San Sebastián, Spain

1

Abstract

Metallorganic molecules have been proposed as excellent spin filters in molecular spintronics because of the large spin-polarization of their electronic structure. However, most of the studies involving spin transport, have disregarded fundamental aspects such as the magnetic anisotropy of the molecule and the excitation of spin-flip processes during electron transport. Here, we study a molecule containing a Co and an Fe atoms stacked between three cyclopentadienyl rings that presents a large magnetic anisotropy and a S=1. These figures are superior to other molecules with the same transition metal, and improves the spin-filtering capacities of the molecule. Non-equilibrium Green's functions calculations based on density functional theory predict excellent spin-filtering properties both in tunnel and contact transport regimes. However, exciting the first magnetic state drastically reduces the current's spin polarization. Furthermore, a difference of temperature between electrodes leads to strong thermoelectric effects that also suppress spin polarization. Our study shows that in-principle good molecular candidates for spintronics need to be confronted with inelastic and thermoelectric effects.

Introduction

Molecular spintronics is a thriving field driven by advances in shrinking electronic devices using molecules[1] and by the extraordinary properties of spin transport.[2,3] Not only are molecules complex enough to attain dedicated functionalities, but they are identically replicated and cheap to manufacture using chemical synthesis. Recently, it has been possible to address individual molecules while taking advantage of their hierarchical growth to create structures of increasing complexity.[4] Molecules can become fundamental pieces of the ever shrinking device technology.[5] Additionally, molecules show a great diversity of magnetic properties that can be successfully tailored, such as spin-crossover molecules,[6] molecular magnets,[3] spin-filtering molecules,[7] molecular spin valves[8] and molecular switches.[7] Molecular spintronics is then a rich field which promises scientific and technological breakthroughs.

An interesting functionality that has been sought after in molecules is the capability of select-

ing one spin to be transmitted in a given spintronic device.[9] In order to achieve this, the molecule presents spin-polarized frontier orbitals, with one of the spins more coupled to the contacting electrodes. In this way, the coupled molecular orbital has a larger contribution to electronic transport, favoring the transmission of one spin species. Typically the molecular spin polarization is achieved by using complexes where the metallic atom (or atoms) present an open-shell configuration. The ligand field of the rest of the molecule on the metallic atoms lead to interesting physics: different spins can be present within the small energy scale of the ligand field.[6] This is particularly true in the case of a sizable spin-orbit coupling (SOC) and a spin larger than 1/2, because the ligand field creates a magnetic anisotropy due to the SOC that can fix the orientation of the molecular spin leading to the appearance of molecular magnets.[10] However, even in the absence of a fixed magnetic-moment orientation, many different molecular systems have been signaled as spin filters, because transport is basically dominated by one of the electron's spins. Indeed, recent works[11,12] show that in the absence of a magnetic center, radical molecules can be used leading to spin-polarized electron transport.

Large spin polarizations have been predicted for the family of molecules made from intercalated sequences of organic rings and transition metals. Examples of these molecules are benzene-vanadium ensembles,[13] benzene-cobalt,[9] cobaltocene[14] and ferrocene and 1-D ferrocene-based wires.[15] Complete studies of different stacking of cyclopentadienyl (Cp) and transition metals (TM) or benzene and transition metals have also been performed.[16,17] Stacking two different TM's has been less common. Some calculations suggest that infinite sequences of stacked TM-Cp present exotic electronic structure with different magnetic ordering depending on the used TM atom.[18] Here, we propose a new molecular spin filter by stacking an iron and a cobalt atom between three cyclopentadienyls (Cp-Fe-Cp-Co-Cp).We performed non-equilibrium Green's functions (NEGF) simulations to evaluate the transport properties of this molecule, $CoFeCp_3$, based on density functional theory (DFT). As expected, the spin polarization obtained in transport approaches 100%. Moreover, the hybrid magnetic structure of this molecule leads to a ferromagnetic coupling between the magnetic centers, where most of the magnetization is localized on the

cobalt atom. Due to the sizable spin-orbit coupling of Co, the Cp ring induce a sizable magnetic anisotropy energy (MAE) which is very interesting for spin-filtering applications. However, this same energy scale sets the energy scale for the first spin excitations that can drastically reduce the spin-polarization in the electron current.[19,20] We evaluate here the effect of bias in reducing the spin polarization as spin-flip processes become energetically accessible.

Our calculations show that transport takes place through the molecular electronic structure based on its π-orbitals. The broken-symmetry electronic structure of $CoFeCp_3$ leads to frontier orbitals of different nature and spin. In contact with metallic electrodes, only the tails of the resonances caused by the molecule-electrode interaction contribute to transport. Hence, transmission changes rapidly with energy near the Fermi energy which should lead to large thermoelectric effects.[21–23] Moreover, the thermoelectric properties should be different per spin, which can lead to spin currents even in the absence of charge currents.[24–26]

Theoretical methods

In order to perform the calculations of this work, we have mainly used two density-functional theory (DFT) packages. VASP[27–32] has been used to explore the adsorption of the $CoFeCp_3$ molecule on the Cu(111) surface and also its magnetic anisotropy. Geometrical effects when a second electrode (another Cu(111) surface) was approached, have been evaluated with VASP. However, the bulk of the calculations has been performed using the SIESTA package.[33] These calculations confirmed the results obtained from VASP and permitted us to perform electronic transport calculations using TRANSIESTA.[34]

We optimized the structure of the $CoFeCp_3$|Cu(111) interface, using density functional theory (DFT) at the spin-polarized generalized gradient approximation (GGA-PBE) level, as implemented in VASP.[27–32] In order to introduce long-range dispersion corrections, we employed the so called DFT-D2 approach proposed by Grimme.[35] We used a plane wave basis set and the projected augmented wave (PAW) method with an energy cut-off of 400 eV. A 19-Å thick vacuum region was

used to decouple the surfaces of consecutive slabs in the supercell approach used in VASP. The surfaces were modeled using a slab geometry with five Cu layers and a $3 \times 2\sqrt{3}$ unit cell. Such an unusual unit cell have been chosen based on experimental data for ferrocene ($FeCp_2$) molecules, which can be seen as one of the building blocks for $CoFeCp_3$. Self-assembled monolayers of ferrocene shows a $6 \times 2\sqrt{3}$ periodicity with two molecules per unit cell.[36] Published calculations yield that these two molecules do not interact between them.[37] Therefore, we decided to carry out our calculations using a smaller $3 \times 2\sqrt{3}$, which is still large enough to prevent interactions among adsorbed molecules.

During the geometry optimizations, we allowed for the relaxation of all atoms of the molecule and of the two-topmost layers of the Cu surface until the atomic forces were smaller than 0.02 eV/Å. A $7 \times 7 \times 1$ k-point sampling of the first Brillouin zone was performed using the Monkhorst-Pack method.[38]

Transport calculations were carried out from first-principles with a method based on nonequilibrium Green's functions (NEGF) combined with DFT as implemented in the TRANSIESTA package.[34] The open-boundary system is divided in three distinct regions breaking the periodicity along the transport direction. The central part is the scattering region and the other two regions are the semi-infinite left and right electrodes, formed by periodically repeating six layers of bulk copper.

The most favorable configuration after geometrical optimization of the $CoFeCp_3$|Cu(111) interface was used to build the scattering region. As illustrated in Fig. 1, the scattering region was composed of one $CoFeCp_3$ molecule connected to two Cu(111) surfaces, left and right, each formed by 8 active layers of a $3 \times 2\sqrt{3}$ cell. It is important to stress that two-probe system geometries were obtained after geometry optimizations using VASP. Dispersion corrections were described through the semi-empirical DFT+D2 scheme. Hence, the role of dispersion forces on the transport results is implicitly considered trough the optimization of the junction's geometry.

For transport calculations, the valence electrons wave functions were expanded in a basis set of local orbitals. A double-ζ plus polarization (DZP) basis set was used to describe the molecular states and and a single-ζ plus polarization orbitals (SZP) basis set for the copper electrodes.

5

Diffuse functions were also included to describe surface electrons. The use of a DZP basis set to describe the molecular states is mandatory in order to yield correct transmission functions. Indeed, a SZP basis set led to a shift of the main molecular peaks of ~ 0.3 eV with respect to the DZP molecular peaks. However, using a DZP for the full system does not alter the transmission functions noticeably. Therefore, the chosen basis set seems to be a good compromise between computational cost and quality. We employed the GGA/PBE functional[39] and norm-conserving Troullier-Martins pseudopotentials.[40] A 11×11 in-plane k-point mesh was adequate to obtain sufficiently accurate transport results.

The spin-polarized electron current I_σ ($\sigma = \uparrow, \downarrow$, denoting majority a minority spin channels respectively) was calculated using the Landauer-Buttiker expression:[41]

$$I_\sigma = \frac{e}{h} \int_{-\infty}^{\infty} \tau_\sigma(\varepsilon, V) \left[f(\varepsilon, \mu_L, T_L) - f(\varepsilon, \mu_R, T_R) \right] d\varepsilon. \tag{1}$$

where $\tau_\sigma(\varepsilon, V)$ is the transmission function for an electron of energy ε and spin σ when the bias voltage between the two electrodes is V. In eq.**??**, $f(\varepsilon, \mu_\nu, T_\nu) = (1 + \exp(\varepsilon - \mu_\nu)/k_B T_\nu)^{-1}$ is the Fermi Dirac distribution of electrode ν ($\nu = L, R$, left and right electrodes respectively) with temperature T_ν and chemical potential μ_ν (note that $V = (\mu_L - \mu_R)/e$). The electron charge is given by e and Planck's constant by h.

In the linear-response regime, I_σ can be approximated as[24]

$$I_\sigma \sim G_\sigma V + G_\sigma S_\sigma (T_L - T_R) \tag{2}$$

where G_σ and S_σ are the spin-dependent conductance and Seebeck coefficient which are calculated at zero bias voltage ($V = 0$) as

$$G_\sigma = \frac{e^2}{h} K_{0\sigma}(E_F, T), \tag{3}$$

and

$$S_\sigma = -\frac{1}{|e|T} \frac{K_{1\sigma}(E_F, T)}{K_{0\sigma}(E_F, T)}, \tag{4}$$

where $E_F = \mu_L = \mu_R$ is the Fermi level and

$$K_{\alpha,\sigma}(E_F,T) = -\int \frac{\partial f(\varepsilon, E_F, T)}{\partial \varepsilon} (\varepsilon - E_F)^\alpha \ \tau_\sigma(\varepsilon, 0) \ d\varepsilon$$

with $\alpha = 0, 1$. The total electronic conductance is given by $G = G_\uparrow + G_\downarrow$.

Finally, the spin-filtering capabilities of the molecular junction is analyzed in terms of the spin polarization of the current, CP, defined as

$$CP = (I_\uparrow - I_\downarrow)/(I_\uparrow + I_\downarrow) \times 100. \tag{5}$$

When both the temperature difference and bias voltage between left and right electrode are zero (i.e. $V = 0$ and $T_L - T_R = 0$) the spin-filtering capacities are evaluated using the spin polarization of the transmission function at the Fermi energy. The corresponding quantity is called spin-filter efficiency[42,43] and is defined as

$$SFE = (\tau_\uparrow(E_{Fermi}, 0) - \tau_\downarrow(E_{Fermi}, 0))/(\tau_\uparrow(E_{Fermi}, 0) + \tau_\downarrow(E_{Fermi}, 0)) \times 100. \tag{6}$$

Results and Discussions

In this section, we analyze and discuss the results obtained for CoFeCp$_3$ as a spin filter in the transport of electrons between two copper electrodes. The section is divided in several subsections to give a thorough view of the properties of this molecular device. The first subsection analyzes the isolated molecule and compares it to related molecules, explaining why CoFeCp$_3$ is a good candidate for a spin-filter device. The second subsection analyzes the adsorbed molecule on Cu(111). The third subsection is devoted to electron transport in the elastic regime in the absence of thermoelectric effects, both for tunneling and high-conductance regimes. The modification of the spin-filtering capacities when spin-flip processes are allowed is evaluated in the following subsection. This section is finished by a detailed account of the effect of thermoelectric effects in the

properties of $CoFeCp_3$ as a spin filter.

Gas-Phase $CoFeCp_3$

As shown in Fig. 1, we considered two types of initial structures for $CoFeCp_3$ molecules: eclipsed and staggered (D_{5h} and D_{5d} symmetries, respectively). In agreement with previous results obtained for ferrocene, $FeCp_2$,[44] the eclipsed conformer is slightly more stable than the staggered one (the computed energy difference is 58 meV).

In both conformers, the ligand field splits the degenerated Co/Fe (TM) d levels into one d_{z^2} (a_1) and two doubly-degenerated $d_{xy} = d_{x^2-y^2}$ (e_2) and $d_{zx} = d_{yz}$ (e_1) orbitals. Depending on their symmetry and energy position, these orbitals mix to a different degree with 2p states of the C atoms. For instance, the highest occupied molecular orbitals (HOMO), for majority (HOMO↑) and minority (HOMO↓) spin channels, schematically shown in Fig. 2, have $\sim 50\%$ TM-e_1 and $\sim 90\%$ TM-e_2 character, respectively. On the other hand, lowest unoccupied orbitals (LUMO) for majority (LUMO↑) and minority spin channels (LUMO↓) (see Fig. 2) present $\sim 50\%$ and 75 % TM-e_1 character, respectively. This picture agrees well with the ligand-field splitting of the d-electron manifold in D_5-symmetry.

The Cp ligands roughly contain one electron. Hence, the TM atoms approximately are in d^6 (Fe) and d^7 (Co) configurations, see Table 1. The lowest-energy conformation corresponds to the low-spin one, hence filling the ligand-splitted d levels for Fe and Co leads to a spin 1 molecule. This is confirmed by our calculations, regardless of the used exchange-and-correlation functional. From this picture, we see that Co will host the spin one, and Fe will have spin zero. This is in agreement with the zero spin of ferrocene. However, cobaltocene ($CoCp_2$) is spin 1/2. The difference stems from the presence of a Cp between Fe and Co in $CoFeCp_3$. Indeed, $CoFeCp_3$ is not a ferrocene plus a cobaltocene. Plotting the spin distribution for $CoFeCp_3$, we confirm the above results: spin is largely localized on the Co atom, and the Fe atom is basically not magnetic.

The large spin-orbit coupling of Co, leads to a sizable MAE induced by the Cp's ligand field. We have evaluated the MAE and we obtain that the Co-Fe axis is a hard axis. This means that the

8

magnetic moment of the molecule lies in a plane parallel to the Cp's. The transversal anisotropy is negligible. Hence the magnetic moment is not fixed in a particular direction in the Cp's plane. The MAE is 1.64 meV for both conformers. This is the energy needed to change the magnetic moment from the easy plane to the hard axis. Since the magnetic moment corresponds to $S = 1$, the molecular ground state is doubly degenerate and formed by the spin components $|S_z| = 1$. The first excited state is $S_z = 0$. Hence, the magnetic moment will be localized in the Cp's plane as long as the bias between electrodes is not large enough to flip the spin from $|S_z| = 1$ to $S_z = 0$ as will be discussed below. These results have been obtained in the gas phase and are, in principle, not valid for the adsorbed molecule. As we will see in the next section, the molecule is basically physisorbed on Cu(111) without charge transfer or any interaction from the substrate other than dispersion forces. Hence, we expect that the gas-phase MAE be a good approximation to the MAE of the spin-filter device.

These data indicate that $CoFeCp_3$ is a small molecule with an important spin that is fixed to a plane contained by the Cp ligands, with a pinning energy (MAE) of 1.64 meV. Hence, the molecule can in principle polarize an electronic current to a direction perpendicular to the axis of the molecule. It is interesting to compare this molecule with similar molecules. Co_2Cp3 or Fe_2Cp_3 will not be good spin filters.[20] The presence of an odd number of Cp leads these molecules to present a low-spin configuration $S = 1/2$, which is not subjected to any magnetic anisotropy and cannot be molecular magnets. Molecules with an odd number of Cp's and only one type of TM atom such as Fe or Co, will probably not be good spin filters either because they show antiferromagnetic coupling with its corresponding $S = 0$ ground state. Infinite chains of CoCp[18] also show antiferromagnetic ordering and hence a $S = 0$ ground state. The case of FeCp chains is more complex. For short molecules, the ground state is the low-spin configuration $S = 0$, however as the chain grows larger, a half-metallic ferromagnet develops that can eventually be an excellent spin filter.[18] Here, we propose something simpler, just a $CoFeCp_3$ molecule.

Table 1: Charge distribution and magnetization for the isolated molecule (evaluated with SIESTA **and Mulliken-charge analysis). Total magnetization is $2\mu_B$ ($S = 1$).**

Element	Total Charge (Mulliken)	Magnetization (μ_B) (Mulliken)
Fe	6.687 (d states= 6.191)	0.513 (d states= 0.475)
Co	7.881 (d states= 7.314)	1.731 (d states= 1.684)
C	62.772	-0.262 (-0.228 Cp in between)
H	14.667	0.018

(a)

(b)
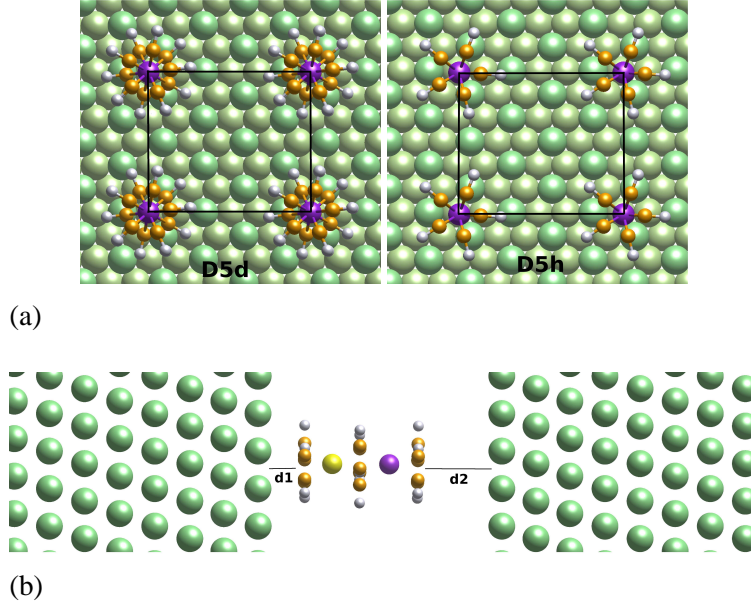
Figure 1: (a) Schematic top view of D_{5d} and D_{5h} conformers within the $3 \times 2\sqrt{3}$ unit cell. Yellow: Fe atom, violet: Co atom, orange: C atoms, grey: H atoms. The black lines represent the surface unit cell. (b) Lateral view of the scattering region used in transport calculations.

Adsorption of CoFeCp$_3$ on Cu(111)

As a first step we carried out full geometry optimizations for a single FeCoCp$_3$ molecule with the Fe-Co axis initially located on the high-symmetry sites of Cu(111): top, bridge, hollow-hcp, and hollow-fcc. The most (least) stable final configuration corresponds to the molecule adsorbed on the hollow (top) site at an average distance of 2.65 Å (2.78 Å) from the surface. However, the energy difference between top and hollow adsorption sites is only 65 meV. Since the computed equilibrium points are spatially very close we do not expect to have large energy barriers between the points, leading to an overall small diffusion barrier.

Charge population calculations using the Bader scheme[45] point to negligible charge transfer between molecule and surface. In addition, neither the geometrical structure nor the electronic characteristic of the molecule seem to be strongly affected by the adsorption process. As a result, the adsorbed molecule maintains its gas-phase electronic and magnetic properties. This is further corroborated by a deep analysis of the contributions to the total adsorption energy.

The main contribution to the adsorption energy, E_{ads}, comes from dispersion forces (E_{vdW}). Indeed, the evaluated adsorption energy on the hollow site is $E_{ads} \sim -1.19$ eV. The contribution to this adsorption energy is mainly due to the van der Waals component, $E_{vdW} \sim -1.28$ eV that is reduced to the final E_{ads} value by the repulsion with the electronic cloud of the surface. Interestingly, if vdW interactions are turned off in the calculations, the molecule feels the repulsive forces and reaches an adsorption distance of 3.22 Å with a very small adsorption energy ($E_{ads} \sim -0.13$ eV) that is probably not meaningful. Nevertheless, these results show that the molecule binds solely by the action of van der Waals forces.

Transport properties of CoFeCp$_3$ on Cu(111)

In the present section, we show the results of our electron transport calculations for a CoFeCp$_3$ molecule between two Cu(111) electrodes with special emphasis on spin filtering. The first results correspond to the electron transmission across the molecular junction at zero bias. First, the tunneling regime is analyzed, where the right electrode is kept at a distance much larger than the adsorption one. Then, we analyze the contact regime, also at zero bias. The third subsection explores bias effect in the more interesting case of the contacted junction. And finally, motivated by the slopes of the transmission function at the Fermi energy, we compute the behavior of the molecular junction with respect to a temperature gradient and the related thermoelectric effects.

All the results of this section have been evaluated for the eclipsed (D_{5h}) molecular conformer. The very similar data about the staggered conformer can be found in the Supporting Information.

Transport in the tunneling regime

Figure 3 (a) shows the transmission spectra at zero bias for a left-(right-)electrode-molecule distance of $d_1 = 2.65$ Å ($d_2 = 5.15$ Å). We approximate the zero-bias conductance by the transmission at the Fermi level, E_F. Hence, the conductance is $G(E_F) = 4.53 \times 10^{-3} G_0$ where $G_0 = 2e^2/h$ is the quantum of conductance. The small value of $G(E_F)$ shows that this setup corresponds to the tunneling regime.

Concerning the effect of the electrodes on the geometry and electronic properties of the molecule, we conclude that it seems to be very small. Within this geometry i) the structural parameters of the molecule are very similar to the ones obtained in gas phase ii) the total charge transfer to the molecule is very modest (0.098 e) and iii) the total magnetization of the molecule is 2 μ_B where the partial contributions coming from Fe, Co, C and H (i.e 0.684 μ_B, 1.567 μ_B, -0.271 μ_B and 0.022 μ_B, respectively) are close to the values reported in Table I for the isolated molecule

Figure 3 shows the extraordinary spin-polarization induced by the molecule. The majority-spin channel transmission ($\tau_\uparrow(E_{Fermi})$) is roughly two orders of magnitude higher than the minority-spin one ($\tau_\downarrow(E_{Fermi})$). As a result, the *SFE* given by eq. **??** approaches 100 % (more precisely, $SFE = 98\%$).

The transmission of Fig. 3 (a) implies that transport is mainly determined by the hybridization of surface electronic states with the frontier molecular orbitals. To get a deeper understanding of the different features observed in the transmission function, we plot the density of states projected (PDOS) onto the frontier orbitals that we analyzed above, namely, the doubly-degenerated HOMO's and LUMO's. These PDOS are depicted in Fig. 3 (b). The PDOS peaks perfectly match the transmission ones, permitting us to identify them.[46] Moreover, we can explain the spin-polarization as due to the different spatial extend of the molecular orbitals in each of the spin channels and the corresponding overlap with the electrodes. Hence, the spin-polarization is rather an effect of the geometry of the molecular orbitals at play rather than due to a spin-polarized density of states.

Projecting the density of states onto atomic orbitals is also instructive. Figure 3 (c) depicts

the PDOS onto the atomic TM-d and Carbon-p states. This permits us to corroborate the above conclusion. Indeed, we can see that while the HOMO↑ has a large component on Carbon-p states, the HOMO↓ is basically a TM-d orbital. This same conclusion, but for different orbitals, is deduced from the LUMO composition.[47] We can then conclude that the larger contribution to the electronic current of the majority spin (↑) orbitals is due to the contribution of Carbon-p states, and hence of the π-orbitals of the Cp ligands revealed in Fig. 2.

Transport in the contact regime

To mimic the contact regime, we approach the right electrode to the molecule at a distance of $d_2 = 2.57$ Å($d_1 = 2.72$ Å).[48] The present electrode configuration has been chosen so as not to exert any pressure on the molecule. Hence, the electrodes induce negligible distortions of the molecular geometrical parameters. The charge transfer to the molecule is still small (0.177 e) and magnetic moment of the molecule reaches 1.895 μ_B (with 0.478 μ_B, 1.630 μ_B, -0.234 μ_B and 0.021 μ_B for Fe, Co, C and H, respectively, which are similar to the ones described in Table 1). Overall, this analysis and the one described for tunneling conditions indicate a modest effect of the electrodes and vdW-forces on the properties of the molecule for the two-probe system.

Figure 4 (a) shows the transmission at zero bias as a function of the electron energy. As expected the transmission is larger than the transmission in the tunneling regime, leading to a total conductance at the Fermi level of $G(E_F) = 0.073G_0$. At the Fermi level, the majority spin channel exhibits a transmission probability one order of magnitude higher than the minority spin channel. Thus, the molecule maintains its spin-filter character ($SFE = 86\%$).

For both spin channels, eigenchannel analysis[49] shows that two scattering states provide the major contribution to the transmission function in the whole energy range. In particular, the two most contributing scattering states provide very similar contributions at the energies corresponding to peaks P1, P2, P3 and P4 (see Fig. 4(b,d)). Although, it is difficult to identify eigenchannels by visualizing them,[50] the perfect energy alignment between these peaks and the ones observed in the PDOS (Fig. 4 (c)) allows again to assign P1 (P2) and P3 (P4) peaks to transmission trough HOMO↑

(HOMO↓) and LUMO↑ (LUMO↓) molecular orbitals. Moreover, assuming Breit-Wigner-like resonances for the transmitting MO, we have fitted the corresponding transmissions with Lorentzian functions[41] which permits us to confirm that the peaks in the transmissions nicely corresponds with the molecular levels in the PDOS (see Supporting Information). Moreover, the Lorentzian fitting, albeit imperfect, shows that the LUMO transmission dominates at the Fermi energy for both spin channels. As the electrode approaches the molecule, the contributions of the LUMOs grow, with no reversal of molecular character in the electron transmission.

As can be seen, the 4 frontier-orbital peaks shift to lower energies with respect to their energy position in the tunneling regime. This is due to the enhancement of the molecule-electrode interactions which also induce a more pronounced broadening of the involved molecular levels. Interestingly, the largest hybridization is observed for P1 where the broadening increases roughly a factor of 6. This behavior can be traced back to the larger overlap of the HOMO↑ with the approaching electrode.

Our transport calculations carried out for the staggered conformer show that the symmetry of the molecule does not affect the spin-filter character of the molecular junction (see Supplementary Information for more details.)

Finite-bias results

The above results imply that FeCoCp$_3$ is a good spin filter in the linear-response regime. In this section, we go beyond the linear-response regime. We computed the electron current for both spin channels ($I_\uparrow$,$I_\downarrow$) as a function of the applied bias using eq. **??**.

Figure 5(a) shows the electron transmission that enters the Landauer equation, eq. **??**, evaluated for three different bias. The upper panel shows the majority spin transmission. We find that the HOMO-LUMO gap increases with bias and the transmission in between the two peaks decreases. For the minority spin (lower panel) the bias effect is negligible. Overall, the effect of the bias is small and using the zero-bias transmissions seems justified. Nevertheless, it is interesting to both understand why the bias effect is small and why the effect is not noticeable for the minority spin.

The effect is small because the molecule is basically bound by dispersion forces, hence the molecular electronic structure presents small perturbations from the electrodes. The presence of an external electrical field acts on the polarization of the molecule. Here, the fields are so small that this effect is negligible. The flowing of a current through the molecule is a larger effect, leading to a change in the steady-state charge of the molecule. However, the HOMO stabilizes by trapping a very small amount of charge and in the same degree the LUMO empties, contributing to an almost zero change in charge state. This leads to a small opening of the HOMO-LUMO gap.

As we have previously seen, the minority-spin molecular orbitals are less coupled to the substrate. Hence, the opening of the HOMO-LUMO gaps is negligible. Interestingly, the effect of the bias on the magnetic moment of the molecule is negligible (i.e it goes from 1.895 μ_B to 1.860 μ_B when the bias increases 0.5 V, see Tables 3-4 in the Supporting Information).

Figure 5(b) shows the current computed using the Landauer equation, eq. **??**. In the linear regime the majority-spin current, $I_\uparrow$ is appreciably larger than $I_\downarrow$ due to the higher conductivity for majority than for minority spin channels ($0.0675G_0$ vs $0.0055G_0$). Such a large difference between $I_\uparrow$ and $I_\downarrow$ is still observed as the voltage further increases. As a result, FeCoCp$_3$ acts as a spin filter in the whole bias voltage range with a large current polarization, CP $\sim$ 84 %. The inclusion of bias in our calculations does not change the conclusion that this molecule is an excellent spin filter with a CP close to 90%.

These results are in contrast with the ones of Ref.[51] where they find that the CP in a Fe-C$_{70}$C$_{70}$-Fe junction goes from 78% at zero bias to 20% at 0.5V. The large difference between our results and theirs can be traced back to the very different interaction of the molecules with the electrodes. While in our case the molecule is physisorbed by van der Waal forces, in their case, a strong covalent interaction rules the charge flow through their Fe-C$_{70}$C$_{70}$-Fe junction.

Spin flip effects

The electronic current can yield energy to the molecular spin degrees of freedom, and hence change the spin state of the molecule. As a consequence spin excitations can reduce the spin-filtering

capabilities of the device if the excited states corresponds to different spin alignments. Let us briefly describe spin transport through the FeCoCp$_3$ molecule.

The MAE of the molecule is 1.64 meV as described above. The molecular axis aligning the Fe and Co atoms is a hard axis. Hence, the molecular ground state corresponds to a spin of 1 in the easy plane described by the Cp ligands which corresponds to a $S_z = 0$ if the molecular axis is taken as the z-axis. In this conditions, the electron spin is contained in the molecular easy plane. As we have seen before, the spin-polarization with respect to an axis on this plane will be very large, well above 80% in all the cases analyzed above. Precession of the spin-polarization axis will be small, and the spin current will be polarized in an arbitrary axis contained in the molecular plane.

A spin Hamiltonian can be written that reproduces the MAE for this $S = 1$ molecule. We can easily see that

$$\hat{H}_{spin} = DS_z^2. \tag{7}$$

In the present case the value of D is 1.64 meV. From here we see that the first excitation is indeed equal to 1.64 meV and it corresponds to flipping the spin from $S_z = 0$ to $|S_z| = 1$, *i.e.* from the easy plane to the hard axis. Hence, electrons with energy above the first-excitation threshold (biases above 1.64 mV) can flip the molecular spin out of the easy plane if they flip their spin. A simple calculation[19] shows that the incoming electron has a probability of 1/3 to flip its spin in the present case. As a consequence the *CP* goes from a value close to 100% to 33% when the absolute value of the applied bias goes above 1.64 mV (in the case where the intrinsic spin-polarization due to the electronic structure is the 84% of the previous section, the spin polarization above the spin-flip threshold becomes 28%).

This description is valid both for the tunneling and the contact transport regimes, since only the molecular MAE and spin multiplicities enter it.

Thermoelectric effects

Motivated by the different ratios τ'_σ/τ_σ at the Fermi level for minority and majority spin channels, we evaluate whether a spin-polarized thermopower current can reduce the spin polarization of the

total current. This is of importance because the spin filtering capacities may not be maintained in the presence of a temperature drop ($\Delta T = T_L - T_R$) across the junction. This physical situation can be reached when the electrodes are contacted in a different way, and current dissipation in the electrodes may lead to different temperatures.

For this purpose, we take a temperature drop $\Delta T = -10K$ between electrodes and compute the spin-polarized electron current, I_σ with $\sigma = \uparrow, \downarrow$ using eq. **??**, for different Bias. The current polarization, CP (eq. **??**), obtained in each case as a function of the average electrode temperature T ($T = (T_L + T_R)/2$) is shown in Fig. 6(a). For the sake of comparison, we plot the CP values obtained when both electrodes are at exactly the same temperature.

At zero ($Bias = 0$) and extremely low bias ($Bias = 2 \times 10^{-6}$ V), we see that thermal effects induce a drop of the CP value from $\sim$86% when both electrodes are at the same temperature to 40-50% in presence of a small temperature gradient. However, the excellent spin-filtering capabilities are restored as soon as the bias voltage is slightly increase; the CP reaches again 86% when the bias is 0.02 V.

To understand such thermal effects on the current polarization, one simply needs to make use of the linear-response limit of the spin polarized electron current which tells us that $I_\sigma = I_\sigma^V + I_\sigma^{th} = G_\sigma V + G_\sigma S_\sigma \Delta T$; $\sigma = \uparrow, \downarrow$ (see eq. **??**). From this expression, we can clearly establish two limiting behaviors: one dominated by thermoelectric current I_σ^{th} at low biases, and the other one by the bias, I_σ^V, when the bias becomes larger than a critical bias, V_c, given by $V_c \approx k_B \Delta T$.

Let us focus on the first case, Fig. 6(b), where I_σ can be approximated by $G_\sigma S_\sigma \Delta T$ ($\sigma = \uparrow, \downarrow$). Here, CP is reduced to $(G_\uparrow S_\uparrow - G_\downarrow S_\downarrow)/(G_\uparrow S_\uparrow + G_\downarrow S_\downarrow)$. Hence, the Seebeck coefficient (S_σ) times the conductance (G_σ) for the two spin channels are the key ingredients of the current polarization. The spin-dependent conductances $G_\uparrow$ and $G_\downarrow$ with average values 5250 nA/V and 409 nA/V, respectively, barely change in the studied temperature window. In addition, the spin-dependent Seebeck coefficient as a function of the electrode temperature plotted in Fig. 6(c) shows that $|S_\uparrow|$ is roughly four times lower than $|S_\downarrow|$. As a result, $|G_\uparrow S_\uparrow|$ is crudely three times larger than $|G_\downarrow S_\downarrow|$ (see Fig. 6(d)) which explains the 40-50 % of current spin polarization observed in Fig. 6(a).

17

With regards to the second case where $I_\sigma \sim G_\sigma V$, the current spin polarization is here simplified to $CP \sim (G_\uparrow - G_\downarrow)/(G_\uparrow + G_\downarrow)$. Therefore, the excellent spin-filtering capacities ($CP = 86\%$) found in this case can be traced back to a much higher conductance for majority than minority spin channels.

Summarizing, thermoelectric effects in this type of molecular junctions lead to a strong suppression of the otherwise excellent spin-filtering properties of the molecules when the electronic transport is governed by the thermoelectric current.

A different thermal effect is the one given by a homogeneous temperature. As the temperature rises, the direction of the molecular spin can change. Indeed, at $\sim$20 K, the ambient temperature is large enough to induce spin flips, similar to the spin-flips we have described in the previous section.

Summary and Conclusions

Using DFT calculations together with a NEGF implementation of electronic transport equations, we have evaluated the gas-phase, adsorption and transport properties of a CoFeCp$_3$. The motivation to do so is the spin (S=1) of the gas-phase molecule, and its magnetic anisotropy (MAE=1.64 meV). These two properties are good characteristics for a tentative molecular-based spin filter.

The molecular spin is largely localized on the Co atom, and the Fe atom is basically not magnetic. This is due to the charge transfer originating in the Cp ligands, and is in agreement with what is found for cobaltocene and ferrocene.

On a Cu(111) surface, we find that the molecule binds via dispersion forces and that the charge transfer is negligible, hence keeping the above molecular properties. The molecules present two conformers, one where the Cp rings are aligned, eclipsed conformer, and a second conformer where the Cp are alternatively rotate in a staggered fashion. We find that systematically the eclipsed conformer is more stable.

The transport properties of the molecules are computed in the tunneling and contact regimes.

On the adsorbed-molecule setup, a second electrode is approached. We have used an electrode-molecule distance of 5.15 Å to characterize the tunneling regime. The contact regime corresponds to a molecule-electrode distance of 2.72 Å. We find that the Fermi energy is in the middle of the HOMO-LUMO gap and that the transmission is largely dominated by the tail of the LUMO resonance. Due to the large contribution of the Cp ligands to the majority-spin HOMO and LUMO we find a large electron transmission for the majority spin channel. At the same time, the electron transmission through the minority-spin channel is smaller due to the prevalence of the TM-d orbitals. As a result, we find a strong spin polarization in the current, with a polarization of 98% in the tunneling geometry and 86% in contact.

When voltage is applied across the molecular junction, we find a small opening of the HOMO-LUMO gap in the majority-spin channel, while a negligible effect for the minority-spin one. The current spin polarization is very constant, changing from the above 86% at 0 V to 83% at 0.5 V. The behavior with bias is very weak due to the weak coupling of the molecule to the electrodes and the negligible charge transfer. However, as the bias increases inelastic channels open that further reduce the spin polarization of the current.

For biases larger than 1.64 mV, equivalent to the MAE of the molecule, electrons can flip the molecular magnetic moment out of the easy plane. As a result the spin of electrons also change and the spin polarization is reduced. For the first excitation threshold this reduces the current polarization to 33%.

Also thermoelectric effects in the absence of applied bias lead to a strong suppression of the otherwise excellent spin-filtering properties of the molecules. When bias is applied, the much larger bias contribution overrides the small thermopower and the spin-filtering properties of the molecular junction are recovered.

In conclusion, a superficial analysis of our calculations would show the triple-decker molecule CoFeCp$_3$ as an excellent current spin filter. However, spin-flip processes and thermocurrents have very negative consequences for this type of device. A negligible temperature difference between electrodes can rapidly diminish the spin-filter efficiency when the electronic transport is governed

by thermoelectric currents. Moreover, ubiquitous spin-flip inelastic effects need to be considered when evaluating the spin-filtering properties of a molecular junction.

Acknowledgments

Supporting Information Available

- Pseudopotential

- Basis Set

- Transport calculations for the D5d (staggered) conformer

- Lorentzian fits to transmissions and molecular contributions to transport

- Mulliken analysis as a function of the applied bias

This material is available free of charge via the Internet at `http://pubs.acs.org/`.

Notes and References

(1) Joachim, C.; Gimzewski, J. K.; Aviram, A. Nature **2000**, 408, 541–548.

(2) Wolf, S. A.; Awschalom, D. D.; Buhrman, R. A.; Daughton, J. M.; von MolnÃąr, S.; Roukes, M. L.; Chtchelkanova, A. Y.; Treger, D. M. Science **2001**, 294, 1488–1495.

(3) Bogani, L.; Wernsdorfer, W. Nature Materials **2008**, 7, 179 – 186.

(4) Barth, J. V.; Costantini, G.; Kern, K. Nature **2005**, 437, 671 – 679.

(5) Raman, K. V.; Kamerbeek, A. M.; Mukherjee, A.; Atodiresei, N.; Sen, T. K.; LaziÄĞ, P.; Caciuc, V.; Michel, R.; Stalke, D.; Mandal, S. K.; BlÃijgel, S.; MÃijnzenberg, M.; Moodera, J. S. Nature **2013**, *493*, 509–513.

(6) Real, J. A.; Gaspar, A. B.; Munoz, M. C. Dalton Trans. **2005**, 2062–2079.

(7) Hao, H.; Zheng, X. H.; Dai, Z. X.; Zeng, Z. Applied Physics Letters **2010**, *96*, 192112.

(8) Urdampilleta, M.; Klyatskaya, S.; Cleuziou, J.-P.; Rube, M.; Wernsdorfer, W. Nature Materials **2011**, *10*, 502–506.

(9) Sen, S.; Chakrabarti, S. J. AM. CHEM. SOC. **2010**, *132*, 15334.

(10) Katoh, K.; Yoshida, Y.; Yamashita, M.; Miyasaka, H.; Breedlove, B. K.; Kajiwara, T.; Takaishi, S.; Ishikawa, N.; Isshiki, H.; et al., Journal of the American Chemical Society **2009**, *131*, 9967–9976.

(11) Herrmann, C.; Solomon, G. C.; Ratner, M. A. Journal of the American Chemical Society **2010**, *132*, 3682–3684, PMID: 20192192.

(12) Herrmann, C.; Solomon, G. C.; Ratner, M. A. The Journal of Chemical Physics **2011**, *134*, 224306.

(13) Koleini, M.; Paulsson, M.; Brandbyge, M. Phys. Rev. Lett. **2007**, *98*, 197202.

(14) Liu, R.; Ke, S.-H.; Yang, W.; Baranger, H. U. The Journal of Chemical Physics **2007**, *127*, 141104.

(15) Zhou, L.; Yang, S.-W.; Ng, M.-F.; Sullivan, M. B.; Tan,; Shen, L. Journal of the American Chemical Society **2008**, *130*, 4023–4027.

(16) Wang, L.; Cai, Z.; Wang, J.; Lu, J.; Luo, G.; Lai, L.; Zhou, J.; Qin, R.; Gao, Z.; Yu, D.; Li, G.; Mei, W. N.; Sanvito, S. Nano Letters **2008**, *8*, 3640–3644, PMID: 18816146.

(17) Bagrets, A. Journal of Chemical Theory and Computation **2013**, *9*, 2801–2815.

(18) Morari, C.; Allmaier, H.; Beiuşeanu, F.; Jurcuţ, T.; Chioncel, L. Phys. Rev. B **2012**, 85, 085413.

(19) Gauyacq, J.-P.; Lorente, N.; Novaes, F. D. Progress in Surface Science **2012**, 87, 63 – 107.

(20) Kepenekian, M.; Gauyacq, J.-P.; Lorente, N. Journal of Physics: Condensed Matter **2014**, 26, 104203.

(21) Cutler, M.; Mott, N. F. Phys. Rev. **1969**, 181, 1336–1340.

(22) Paulsson, M.; Datta, S. Phys. Rev. B **2003**, 67, 241403.

(23) Reddy, P.; Jang, S.-Y.; Segalman, R. A.; Majumdar, A. Science **2007**, 315, 1568–1571.

(24) Cornaglia, P. S.; Usaj, G.; Balseiro, C. A. Phys. Rev. B **2012**, 86, 041107(R).

(25) Luo, B.; Lü, J.-T.; Gao, J.-H.; Yao, K.-L. Scientific Reports **2014**, 4, 4128.

(26) Yang, X. F.; Liu, Y. S.; Zhang, X.; Zhou, L. P.; Wang, X. F.; Chic, F.; Feng, J. F. Phys. Chem. Chem. Phys. **2014**, 16, 11349.

(27) Kresse, G.; Hafner, J. Phys. Rev. B **1993**, 47, 558.

(28) Kresse, G.; Hafner, J. Phys. Rev. B **1993**, 48, 13115.

(29) Kresse, G.; Furthmüller, J. Comput. Mater. Sci. **1996**, 6, 15.

(30) Kresse, G.; Furthmüller, J. Phys. Rev. B **1996**, 54, 11169.

(31) Kresse, G.; Joubert, D. Phys. Rev. B **1999**, 59, 1758.

(32) Hafner, J. J. Comput. Chem. **2008**, 29, 2044–2078.

(33) Soler, J. M.; Artacho, E.; Gale, J. D.; GarcÃ■a, A.; Junquera, J.; OrdejÃşn, P.; SÃąnchez-Portal, D. Journal of Physics: Condensed Matter **2002**, 14, 2745.

(34) Brandbyge, M.; Mozos, J.; Ordejon, P.; Taylor, J.; Stokbro, K. Phys. Rev. B **2002**, 65, 165401.

(35) Grimme, S. J. Comput. Chem. **2006**, 27, 1787.

(36) Heinrich, B.; Limot, L.; Rastei, M.; Iacovita, C.; Bucher, J. P.; Djimbi, D. M.; Massobrio, C.; Boero, M. Phys. Rev. Lett. **2011**, 107, 216801.

(37) Ormaza, M.; Abufager, P.; Bachellier, N.; Robles, R.; Verot, M.; Bahers, T. L.; Bocquet, M.-L.; Lorente, N.; Limot, L. J. Phys. Chem. Lett. **2015**, 6, 395âĂŞ400.

(38) Monkhorst, H.; Pack, D. Phys. Rev. B **1976**, 13, 5186.

(39) Perdew, J. P.; Burke, K.; Ernzerhof, M. Phys. Rev. Lett. **1996**, 77, 3865.

(40) Troullier, N.; Martins, J. L. Phys. Rev. B **1991**, 43, 1993.

(41) Datta, S., Ed. Electronic Transport in Mesoscopic Systems; Cambridge University Press, Cambridge, 1995.

(42) Wu, J.-C.; Wang, X.-F.; Zhou, L.; Da, H.-X.; Lim, K. H.; Yang, S.-W.; Li, Z.-Y. J. Phys. Chem. C **2009**, 113, 7913.

(43) Maslyuka, V. V.; Achilles, S.; Mertig, I. Solid State Communications **2010**, 150, 505.

(44) Mohammadia, N.; Ganesana, A.; Chantler, C. T.; Wang, F. Journal of Organometallic Chemistry **2012**, 713, 51.

(45) Tang, W.; Sanville, E.; Henkelman, G. Journal of Physics: Condensed Matter **2009**, 21, 084204.

(46) The clear correspondence between peaks (marked P1, P2, P3 and P4 in Fig. 3 (a)) on the transmission function and the PDOS, Fig. 3 (b-c), makes it possible to assign P1 at -0.61 eV (P2 at -0.67 eV) and P3 at 1.18 eV (P4 at -1.42 eV) peaks to the transmission trough HOMO↑ (HOMO↓) and LUMO↑ (LUMO↓), respectively. The Fermi level is found to lie closer to HOMO states than LUMO states for both spin channels. However, the linear-response regime

is controlled by the LUMO of both spins. We expect then that a low-bias scanning tunneling microscope image will be an image of the molecular LUMO.

(47) The narrower-width and lower-height peak found for P2 as compared to the P1 one can be understood by close inspection of the involved molecular orbitals. As it was previously discussed, HOMO↓ (P2) is basically an e_2 orbital ($d_{xy} - d_{x^2-y^2}$ perpendicular to the transport direction) orbital with its electronic cloud completely localized on the TM-centers, this leads to a poor hybridization with the electrodes and low transmission probability. On the other hand, the HOMO↑ (P1) is more delocalized and it is built from e_1 (d_{xz}, d_{yz}) TM-d orbitals. As a result its hybridization with the electrodes as well as its transmission probability are higher. Concerning peaks P3 and P4, it is interesting to note that although both show similar transmission probabilities, the P3 structure has a much broader energy range than the P4 one. Such features can be understood taking into account that although, LUMO↑ (P3) and LUMO↓ (P4) are both built from TM-d(e_1) orbitals, LUMO↓ is much more localized about the TM-centers. As a result, its hybridization with the surface electrodes is lower than for the LUMO↑.
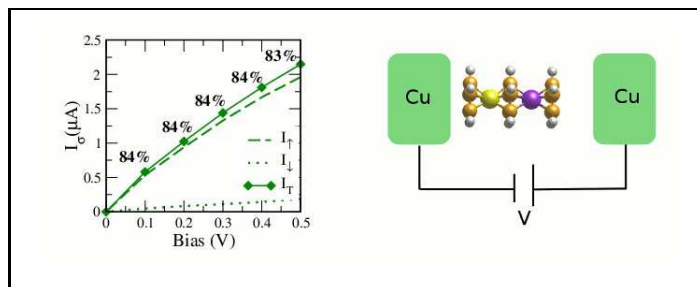
(48) This configuration is 0.01 eV more stable than the one with $d_1 = d_2 = 2.65$ Å where 2.65 Å is the average distance of the molecule on the surface.

(49) Paulsson, M.; Brandbyge, M. Phys. Rev. B **2007**, 76, 115117.

(50) Due to the fact that the eigenvalues of the transmission function corresponding to eigenchannels at $k_{xy} = (0,0)$ do not provide the major contribution to the total transmission.

(51) Cakir, D.; Otalvaro, D. M.; Brocks, G. Phys. Rev. B **2014**, 89, 115407.

Graphical TOC Entry

doubly-degenerated HOMO-majority spin

doubly-degenerated HOMO-minority spin

doubly-degenerated LUMO-majority spin
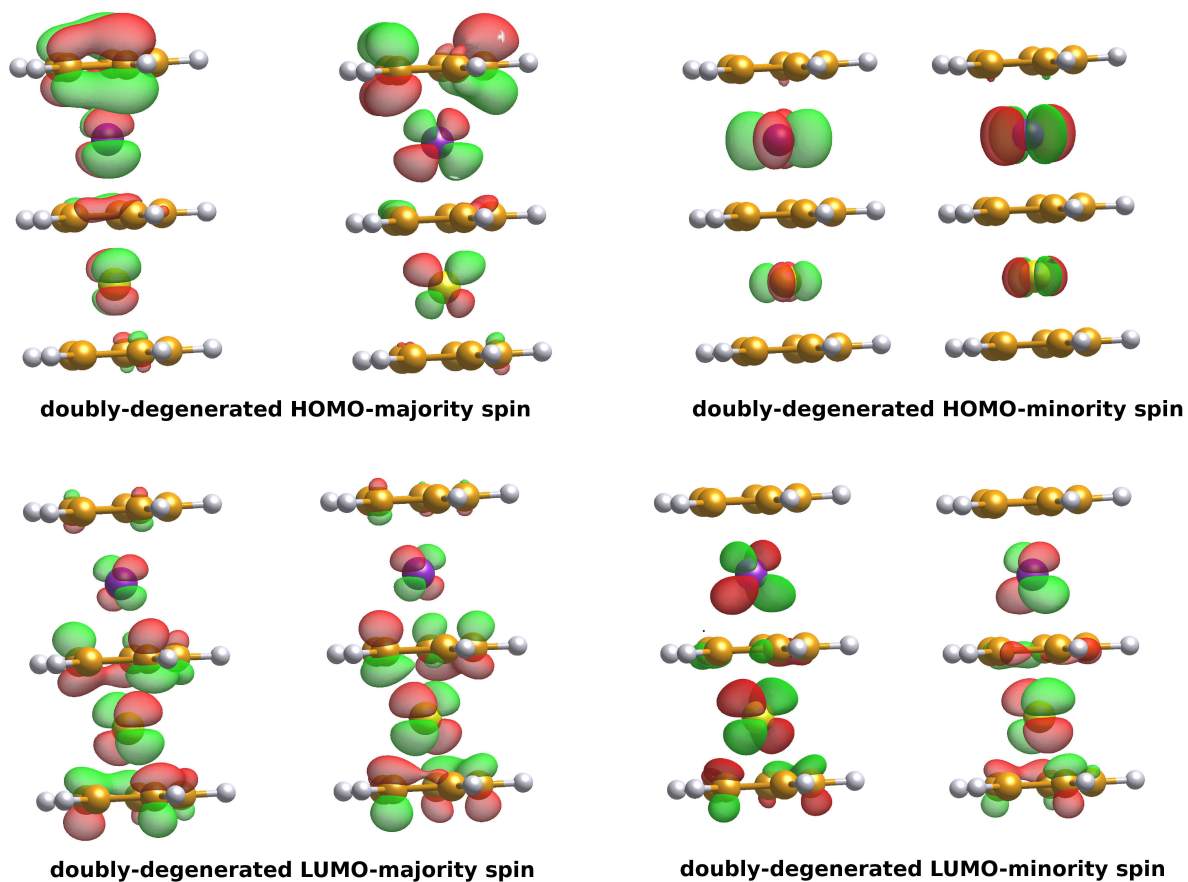
doubly-degenerated LUMO-minority spin

Figure 2: Doubly-degenerated frontier molecular orbitals for the D_{5h} conformer. Plotted isovalues are 10 % of the maximum ones. Red (green) indicates positive (negative) values of the real part of the wavefunction.
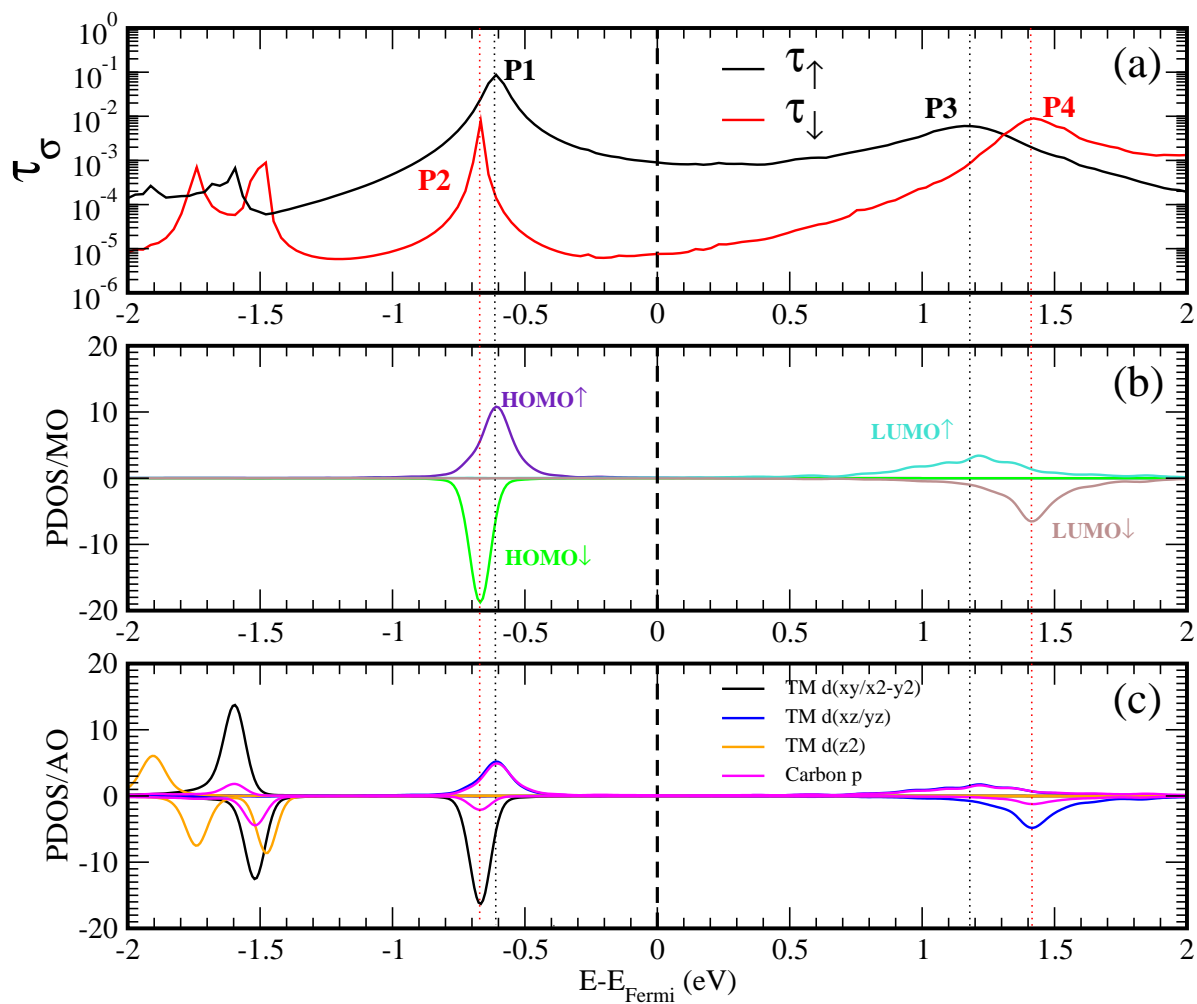
Figure 3: (a) Electron transmissions from the left to the right electrode as a function of electron energy referred to the Fermi energy. (b)Computed spin-polarized PDOS onto frontier molecular orbitals. (c) Computed spin-polarized PDOS projected onto TM-d and Carbon-p atomic orbitals. Tunneling regime d_2=5.15 Å. Total magnetization= 2 μ_B. Mulliken charge transfer to the molecule = 0.098 e
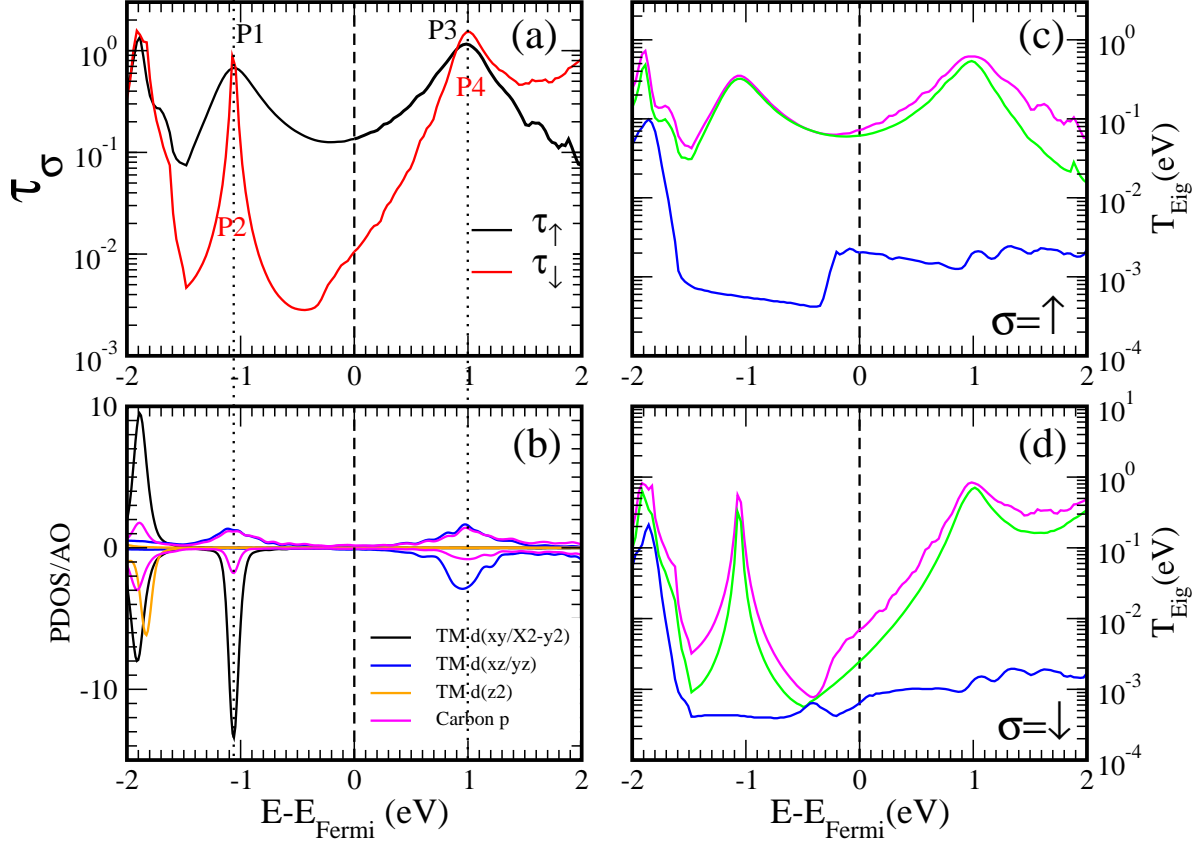
Figure 4: Contact regime $d_2 \sim 2.57$Å. (a) Electron transmissions from the left to the right electrode as a function of electron energy referred to the Fermi energy. (b) the PDOS onto TM-d and Carbon-p states. (c-d) Eigenchannels contribution to the average transmission for majority and minority spin channels (the color-code only denotes the ordering of the transmission eigenvalue at each electron energy and may not be connected to the symmetry or other common properties of the eigenchannels).Total magnetization=$1.92\mu_B$. Mulliken charge transfer to the molecule = $0.177\ e$.
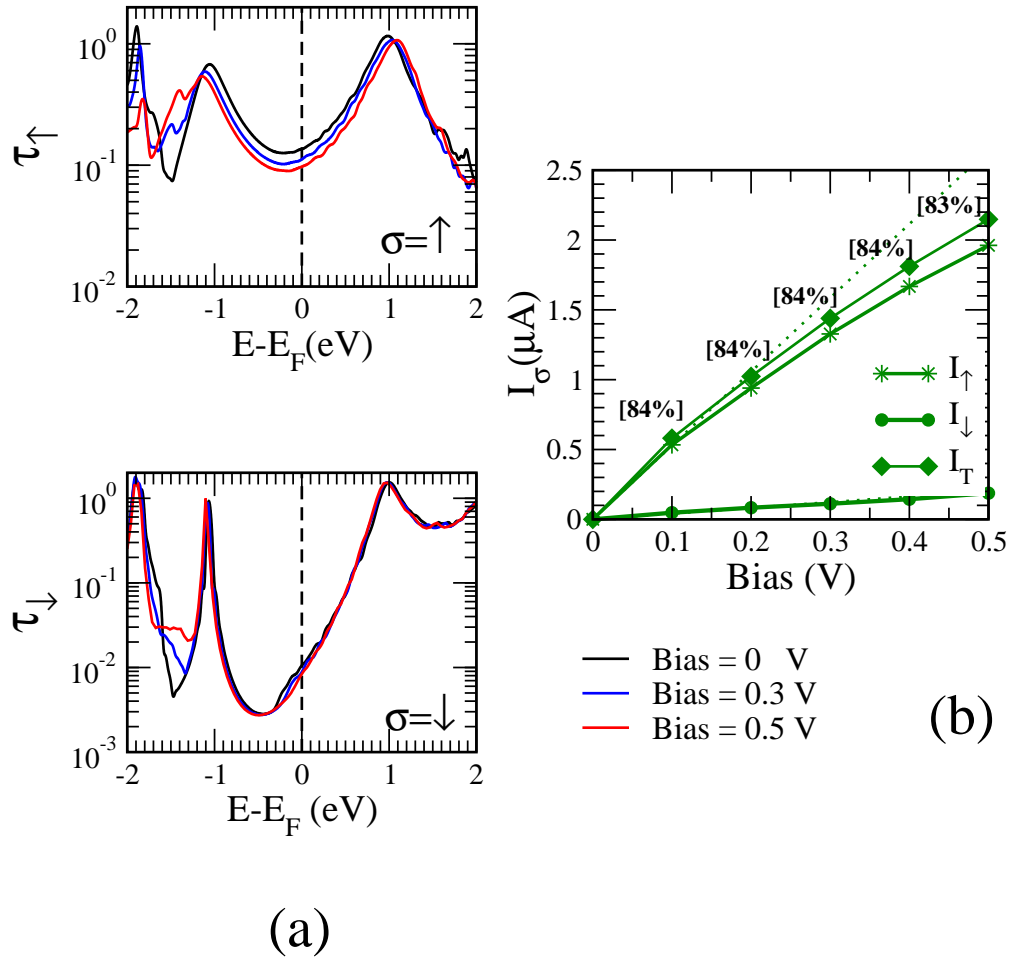
Figure 5: (a) Electron transmission as a function of electron energy for 0, 0.3 and 0.5 V applied between the two metallic electrodes. The majority spin (upper panel) shows that the HOMO-LUMO gap is broadened as the bias is increased and there is a small drop of transmission at the Fermi energy. For the minority spin (lower panel) the shifts are negligible and there is a very minor bias dependence. (b) I-V characteristics in nA and V. The SFE is shown in brackets. Dot lines indicates the results obtained with the linear approach $I_\sigma = G_\sigma V$
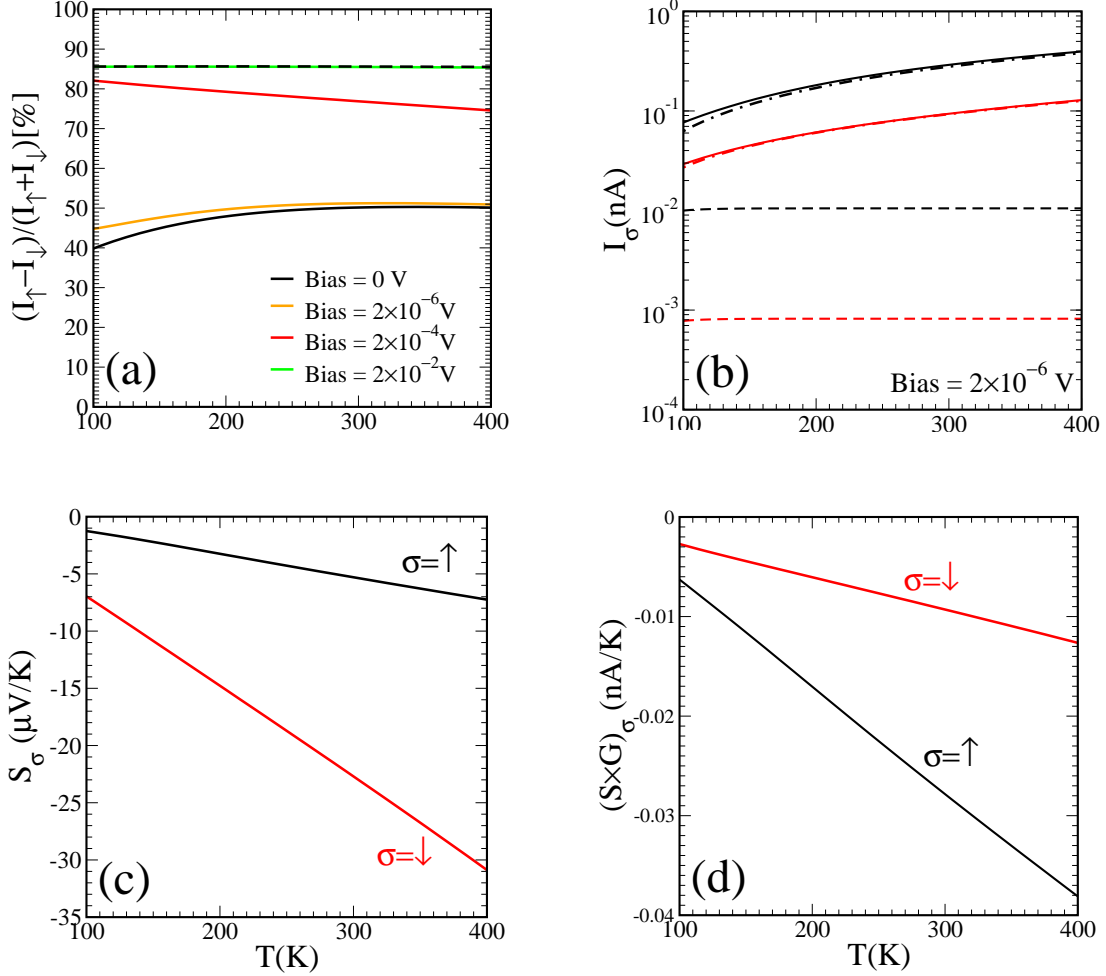
Figure 6: (a) Current polarization (CP) as a function of the average electrode temperature T (i.e. $T = (T_L + T_R)/2$) for different Bias when $\Delta T = -10K$. The black dash line indicates the CP values obtained when both electrode are at exactly the same temperature. (b) Majority (black lines) and minority (red lines) spin polarized currents for an applied bias of 2×10^{-6}V ($\Delta T = -10K$). Dash and dash-dot lines indicates I_σ^V and I_σ^{Th} contributions to the spin-polarized current I_σ shown in solid lines; $\sigma = \uparrow, \downarrow$ (see text). (c) Spin dependent Seebeck coefficient S_σ (μV/K) as a function of the temperature (K). (d) The Seebeck coefficient times the linear conductance (nA/K) for the two spins as a function of the temperature (K).